

Article type : Research Article

# Synthesis, Photophysical and Computational Study of Novel Coumarin Based Organic Dyes

Mahadev N. Kumbar<sup>1</sup>, Madivalagouda S. Sannaikar<sup>2</sup>, Saba Kauser J. Shaikh<sup>1</sup>, Atulkumar  
A. Kamble<sup>1</sup>, Manjunath N. Wari<sup>2</sup>, Sanjeev R. Inamdar<sup>2</sup>, Qiquan Qiao<sup>3</sup>, Bhavya N. R<sup>4</sup>,  
Mahendra M<sup>4</sup>, Jagadeesh Prasad D<sup>5</sup> and Ravindra R. Kamble<sup>\*1</sup>

<sup>1</sup> Department of Chemistry, Karnatak University, Dharwad-580003, Karnataka, India.

<sup>2</sup> Laser Spectroscopy Lab and UGC-CPEPA Programme, Department of Physics, Karnatak  
University, Dharwad -580003, Karnataka, India.

<sup>3</sup> Centre for Advanced Photovoltaics, Department of Electrical Engineering and Computer  
Science, South Dakota State University, Brookings, SD,57007, USA.

<sup>4</sup> Department of Studies in Physics, Manasagangothri, University of Mysore, Mysore - 570006  
Karnataka, India.

<sup>5</sup> Department of Chemistry, Mangalore University, Mangalagangothri-574199, Karnataka, India.

\*Corresponding author email: kamchem9@gmail.com (Ravindra R. Kamble)

## ABSTRACT

A series of novel coumarin pyrazoline moieties combined with tetrazoles, *3-(1-phenyl-4-(1H-tetrazol-5-yl)-1H-pyrazol-3-yl)-2H-chromen-2-one*, *6-chloro-3-(1-phenyl-4-(1H-tetrazol-5-yl)-*

This article has been accepted for publication and undergone full peer review but has not been through the copyediting, typesetting, pagination and proofreading process, which may lead to differences between this version and the Version of Record. Please cite this article as doi:

10.1111/php.12852

This article is protected by copyright. All rights reserved.

*1H-pyrazol-3-yl)-2H-chromen-2-one*, *6-bromo-3-(1-phenyl-4-(1H-tetrazol-5-yl)-1H-pyrazol-3-yl)-2H-chromen-2-one* and *6-bromo-3-(1-(4-bromophenyl)-4-(1H-tetrazol-5-yl)-1H-pyrazol-3-yl)-2H-chromen-2-one* **7(a-d)** were designed and synthesized. Single crystal X-ray diffraction and their interactions were studied by Hirshfeld Surface Analysis. Thermal stabilities and electrochemical properties of these compounds were examined from Differential Scanning Calorimetry (DSC), Thermo gravimetric (TGA) and Cyclic Voltametric (CV) studies. Their spectroscopic properties were analysed in various alcohols and general solvents by UV-Vis absorption, fluorescence and time resolved spectroscopy. In addition, the ground and excited state electronic properties were investigated using density functional theory (DFT). The calculated highest occupied molecular orbital (HOMO) and lowest unoccupied molecular orbital (LUMO) and energy band gap ( $E_g$ ) values have revealed the effect of substitution of halogens. The substitution has equally affected the ground and excited states of **7(a-d)** compounds. The solvatochromism on absorption, fluorescence spectra and fluorescence lifetimes of these compounds were investigated. All these results showed the chromen-2-one of pyrazoline tetrazole derivatives could play an important role in photonic and electronic devices.

## INTRODUCTION

Fluorescent heterocyclic compounds are of huge interest as useful materials and have received increasing attention in recent years due to their wide spread practical applications such as fluorescence sensors and biological imaging, molecular probes used for biochemical research, organic light-emitting diodes (OLEDs) and emitters of electroluminescence devices (1). In the present scenario, OLEDs tend to revolutionize the display technologies in the field of optoelectronics (2,3). Also there are many reports on using fluorescent compounds in

biochemical and medical research (4,5). Since fluorescent dyes exhibit attractive properties, these dyes are carefully integrated with designed functional groups to induce an intended reaction for the generation of the highly fluorescent device (6). However, fluorescent molecules still have unresolved complications such as operational stability of the devices and colour shift after the operation. These problems can be resolved by introducing different substituent to the structure backbone and hence the steric functionalization of the core organic moiety is necessary (7).

Synthetic strategies and the fluorescent nature of coumarin derivatives have been thoroughly reviewed and a worth of coumarin analogs have been studied for absorbance, emissive properties and applications in optoelectronic devices like well known coumarin based dyes; C151, C120, C343, NKX-2311, NKX-2586, NKX-2753 and NKX-2593 (8,9). Considering the high photostability and strong fluorescence of coumarin derivatives,  $\pi$ -extended coumarins are expected to provide several advantageous features over the corresponding coumarins (10,11). Pyrazole and coumarin containing derivatives are used extensively as fluorescence probes for their excellent photophysical properties of high fluorescence quantum yield and efficient membrane permeability. Therefore, we designed a chemosensor due to tetrazole with an active proton, which were combined via intramolecular hydrogen bond upon interaction with various alcohols and general solvents, the intramolecular hydrogen bond was broken and tetrazole anion were formed, which induced its optical changes from weak fluorescence to strong fluorescence. Some of the representative derivatives are presented in Fig. 1.

<Fig. 1 >

Therefore herein, the synthesis of four compounds was accomplished with electron withdrawing substituent (halogens), especially on 6<sup>th</sup> and 4<sup>th</sup> position of coumarin and phenyl

rings, respectively. Due to the importance of these dyes, we have initiated to study the photophysical properties. These tetrazole derivatives of coumarins yield enhanced photoluminescence (PL) and exhibited fluorescence in the blue region (~ 450 nm). This highlights the importance of substituent selection in determining the photophysical properties (12-14), high quantum yield (QY) and also electron transporting materials in OLEDs. However, the photochemical and photophysical properties of intramolecular, electron donor-acceptor systems depend on the excited state processes that occur after absorption of a photon by interacting with surrounding various alcoholic and general solvent molecules (15-17). In such case, rapid electron transfer from donor to acceptor takes place by  $n-\pi^*$  conjugated systems (18-20).

Therefore, we systematically investigated photophysical, electrochemical and thermal properties of novel synthesised compounds by CV, DSC, TGA, time-resolved fluorescence decay, QY, HOMO-LUMO and energy band gap ( $E_g$ ) calculations with a view to examine their suitability in developing an electroluminescence device. Further, we report the effects of solvents polarity (solvatochromism) on absorption and fluorescence spectra to explore strong intramolecular charge transfer (ICT) properties of synthesized dyes. All these results showed tetrazole derivatives of coumarins exhibit good electronic, photophysical and optoelectronic properties.

## **MATERIALS AND METHODS**

*Materials, methods and instruments.* All the reagents and solvents used were of analytical grade purchased from Sigma-Aldrich and E-Merck and used without further purification. IR spectra were recorded in KBr and determined on a disc matrix using an IMPACT-410 Nicolet (USA) Fourier transform infrared spectroscopy (FTIR). Progress of the reaction was checked by Aluchrosep Silica

Gel 60/UV 254 TLC on silica gel coated plates in ethyl acetate and hexane (3:7, 30%) as eluent. The  $^1\text{H}$  and  $^{13}\text{C}$ -NMR spectra were recorded on Bruker Avance 300-MHz FT NMR spectrometers with (DMSO- $d_6$ ) as solvent and tetramethylsilane (TMS) as internal standard. The mass spectra were recorded on Shimadzu GC-MS instrument operating at 70 eV spectrometer and elemental analyses were carried out using Heraus CHN rapid analyzer.

*Steady State and Time Resolved Measurements.* The steady state absorption and fluorescence spectral measurements of samples at room temperature were performed by UV-Vis Spectrophotometer (Hitachi-2800) and Spectrofluorometer (Jobin Yvon Horiba, Fluoromax-4), respectively. And time resolved measurements were conducted by Time Core related Single Photon Counting (TCSPC) instrument (ISS ChronosBH) and data were analysed with Vinci Analysis fitting software.

*Computational details.* The ground and first excited state molecular geometry of the synthesized dyes were optimized by DFT (B3LYP) calculations and configuration interaction singles (CIS) with the 6-31G basis set as implemented in the Gaussian 09 (version D.01) program package. The TD-DFT calculations for the compounds were performed by using B3LYP/6-31G and using triple zeta functions B3LYP/6-31G\*. And also the results were checked against the functional dependence by using CAM-B3LYP and B3PWC91 functional.

*X-ray crystal analysis.* The X-ray diffraction structure measurements were carried out using Bruker SMART CCD area-detector with monochromatic Mo  $K\alpha$  radiation at room temperature. The raw data frameworks were unified with the SAINT (21) program by using a narrow-frame algorithm.

The structures were solved by direct methods and refined by full-matrix least-squares methods on  $F^2$  using *SHELXL* (22) in anisotropic approximation for all non-hydrogen atoms.

*Hirshfeld Surface Analysis.* The application of Hirshfeld surface has been increasing in the field of

crystallography. This approach is a convenient tool for the investigation of intermolecular interactions, because the crystal structure provides the most definite understanding of the intermolecular contacts and crystal packing feature (compound **7b** and **7c**). Hirshfeld surface based tools also appear to be particularly suitable for visualizing variations in the intermolecular interactions of crystals. Hirshfeld surfaces and their associated fingerprint plots were generated using Crystal Explorer 3.1 software (23) from the crystal structure coordinates supplied in the format of Crystallographic Information File (CIF). Tonto, a program feature of Crystal Explorer was implemented to generate a map of electrostatic potential on the Hirshfeld surface by using ab initio Hartree Fock (HF) method with STO-3G basis set (24).

*Thermal properties of synthesized compounds.* Thermal stabilities of synthesized compounds were examined by DSC then data were obtained using standard aluminium pans with heating rates of  $10^{\circ}\text{C min}^{-1}$  from 40 to  $400^{\circ}\text{C}$ , unless otherwise stated. The TGA experiments were recorded with Perkin-Elmer Thermal Analysis at heat rate from 40 to  $700^{\circ}\text{C}$  at  $10^{\circ}\text{C/min}$  in a platinum pan.

*Electrochemical Analysis.* The cyclic voltametry is one of the standard techniques used for electrochemical investigation. The CV experiments were performed by using ACM instrument gill AC 660 potentiostat equipped with a conventional three electrodes (Ag/AgCl couple and platinum plate were reference electrode and auxiliary electrode) at a scan rate of  $50\text{ mV/s}$  at room temperature under  $\text{N}_2$  atm. The setup is computer controlled consisting of a potentiostat VoltaLab 40. Tetrabutylammonium perchlorate in anhydrous acetonitrile ( $\text{CH}_3\text{CN}$ ) was used as electrolyte solution (0.1M).

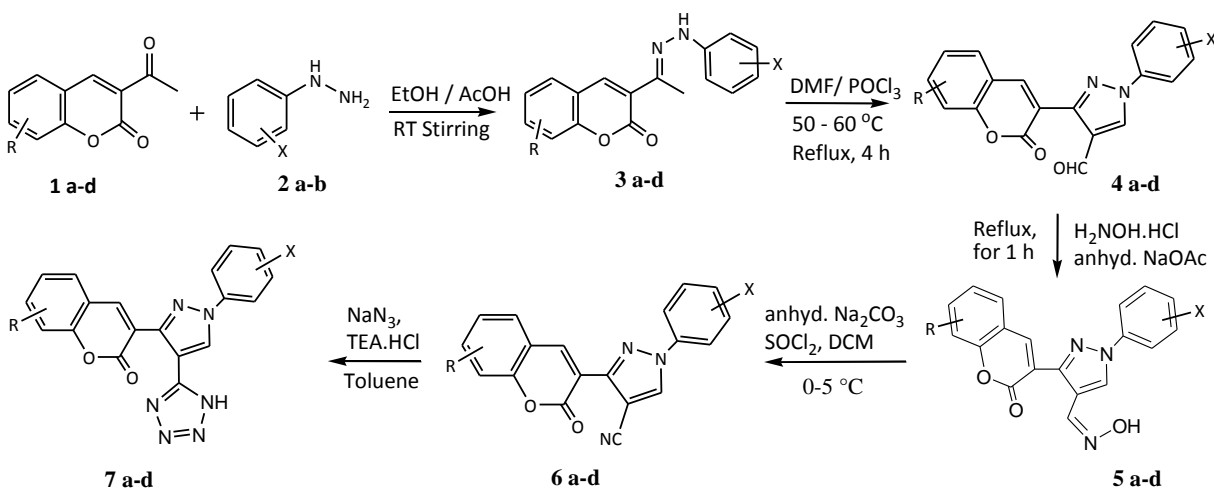
*Synthesis.* 3-(2-Oxo-2H-chromen-3-yl)-1-phenyl-1H-pyrazole-4-carbaldehydes **4(a-d)** were prepared according to the literature method (25).

*Procedure for the conversion of carbaldehyde 4(a-d) into oximes 5(a-d).* A mixture of compound

**4(a-d)** (0.50 gm, 0.0018 m mol) in ethanol (12 ml) was taken in RB flask (25 ml). To this, hydroxylamine hydrochloride (1 gm, 0.0035 m mol) and anhydrous sodium acetate (1.50 gm, 0.054 m mol) were added. Then reaction mixture refluxed for 1h. After completion of the reaction (TLC), reaction mixture was cooled to room temperature and poured into ice cold water. The solid thus obtained was filtered, washed with water and recrystallized from ethanol to get pure crystals of **5(a-d)**.

*Procedure for the conversion of oximes 5(a-d) into nitriles 6(a-d).* Finely powdered  $\text{Na}_2\text{CO}_3$  (0.16 gm, 1m mol) was then mixed with thionyl chloride (2.20 ml, 1m mol) in a RB flask (25 ml) at 0-5°C. To the resulting powder, a solution of oxime (**5a-d**, 1m mol) in dry  $\text{CH}_2\text{Cl}_2$  (15 ml) was slowly added and stirred at 0°C for 1 h. The progress of the reaction was monitored by TLC. After completion of the reaction, the mixture was shaken with DCM (5 ml) and filtered. The residue was further washed with DCM and solvent was evaporated under reduced pressure to afford the final product **6(a-d)**.

*Synthesis of 3-(1-aryl-4-(1H-tetrazol-5-yl)-1H-pyrazol-3-yl)-2H-chromen-2-one 7(a-d).* A mixture of 3-(2-oxo-2H-chromen-3-yl)-1-aryl-1H-pyrazole-4-carbonitrile, **6(a-d)** (0.50 gm, 0.003 m mol),  $\text{NaN}_3$  (0.90 gm, 0.0134 m mol) and tri-ethylamine hydrochloride (1.90 gm, 0.0134 m mol) in toluene (10.00 ml) was heated to 105-110°C for 48 h with constant stirring. The reaction mixture was cooled to room temperature and stirred for 30 minutes at RT. The product was extracted with water (15ml) and NaOH solution (5%, 2ml). Dil. HCL was added drop-wise, the solid thus obtained was filtered to get a pure tetrazole derivative **7(a-d)**.



Where, **7a**; R = -H, X = -H, **7b**; R = -6Cl, X = -H, **7c**; R = -6Br, X = -H, **7d**; R = -6Br, X = -4Br

**Scheme 1** Synthetic approach for target compounds **7(a-d)**.

The synthetic route of the target compounds is outlined in Scheme 1. Initial cyclization of aryl hydrazones **3(a-b)** of 3-acetylcoumarin **1(a-d)** by *Vilsmeier–Haack* reaction afforded a 3-(2-oxo-2H-chromen-3-yl)-1-phenyl-1H-pyrazole-4-carbaldehydes **4(a-d)**. These on reaction with hydroxylamine hydrochloride in presence of anhydrous sodium acetate (NaOAc) under reflux gave oximes **5(a-d)**. Further, these oximes **5(a-d)** were converted into nitriles by thionyl chloride (SOCl<sub>2</sub>) and anhydrous Na<sub>2</sub>CO<sub>3</sub> in DCM (CH<sub>2</sub>Cl<sub>2</sub>) under cold condition to afford coumarin pyrazolo nitriles **6(a-d)**. 1,3-Dipolar cyclization of these nitriles **6(a-d)** with sodium azide in the presence of TEA.HCl (phase transfer catalyst and base) at 105-110°C in toluene gave the title compounds 3-(1-aryl-4-(1H-tetrazol-5-yl)-1H-pyrazol-3-yl)-2H-chromen-2-ones **7(a-d)**. Such newly synthesized compounds were characterized by IR, <sup>1</sup>H and <sup>13</sup>C NMR, Mass spectral and elemental analyses (see Supporting Information).

*Spectral characterizations.*

***(E)-2-(6-Bromo-2H-chromen-2-one)-1-(1-(4-bromophenyl)ethylidene)hydrazine (3d)***

Yield: 82%, colour: pale yellow. MP = 272-274°C (dec.). IR (KBr,  $\nu_{\max}$ ,  $\text{cm}^{-1}$ ): 1707 (coumarin, C=O), 3481 (N-H).  $^1\text{H}$  NMR (400 MHz, DMSO- $d_6$ ):  $\delta$  8.78 (s, 1H, coumarin C<sub>4</sub>-H), 8.42 (s, 1H, Ar-H), 8.42 (s, 1H, N-H), 8.24-7.72 (m, 4H, Ar-H), 7.49 (d, 1H, Ar-H), 7.39 (d, 1H, Ar-H), 1.22 (s, 3H, CH<sub>3</sub>) ppm.  $^{13}\text{C}$  NMR (100 MHz, DMSO- $d_6$ ):  $\delta$  156.63 (coumarin C=O), 152.27, 145.31, 144.22, 143.14, 136.45, 131.99, 131.43, 128.55, 122.40, 120.29, 120.21, 118.65, 118.26, 118.12, 34.10 (CH<sub>3</sub>) ppm. MS-EI, ( $m/z$ ): = 437 [M+4], 435 [M=2], 433.92 [M]; Anal. For C<sub>19</sub>H<sub>12</sub>N<sub>6</sub>O<sub>2</sub>: calcd. C, 46.82; H, 2.77; N, 6.42; Found: C 46.85, H 2.80, N 6.46.

***3-(7-Bromo-2-oxo-2H-chromen-3-yl)-1-(4-bromophenyl)-1H-pyrazole-4-carbaldehyde (4d)***

Yield: 87%, colour: Pale brown. MP = 256-258°C (dec.). IR (KBr,  $\nu_{\max}$ ,  $\text{cm}^{-1}$ ): 1736 (coumarin, C=O), 1678 (pyrazole, C=O).  $^1\text{H}$  NMR (400 MHz, DMSO- $d_6$ ):  $\delta$  9.28 (s, 1H, pyrazole, C-H), 8.45 (s, 1H, coumarin C<sub>4</sub>-H), 8.42 (d, 2H, Ar-H), 7.97-7.69 (m, 4H, Ar-H), 7.51 (d, 1H, Ar-H), 7.44 (d, 1H, Ar-H) ppm.  $^{13}\text{C}$  NMR (100 MHz, DMSO- $d_6$ ):  $\delta$  162.41 (coumarin C=O), 158.43, 155.76, 148.74, 145.12, 138.82, 135.97, 133.64, 131.52, 128.45, 126.48, 125.36, 124.20, 122.61, 120.26, 119.86, 119.54, 118.63, 118.83 ppm. MS-EI, ( $m/z$ ): = 476 [M+4], 474 [M=2], 472 [M]; Anal. For C<sub>19</sub>H<sub>10</sub>Br<sub>2</sub>N<sub>2</sub>O<sub>3</sub>: calcd. C, 48.13; H, 2.13; N, 5.91; Found: C 48.15, H 2.16, N 5.96.

***1-(4-Chlorophenyl)-3-(2-oxo-2H-chromen-3-yl)-1H-pyrazole-4-oxime (5b)***

Yield: 78%, colour: brown. MP = 268-270 °C (dec.). IR (KBr,  $\nu_{\max}$ ,  $\text{cm}^{-1}$ ): 1728 (coumarin, C=O), 3285 (-OH).  $^1\text{H}$  NMR (400 MHz, DMSO- $d_6$ ):  $\delta$  9.09 (s, 1H, pyrazole, C-H), 8.80 (s, 1H, coumarin C<sub>4</sub>-H), 8.32 (d, 1H, Ar-H), 8.06 (s, 1H, Ar-H), 7.93-7.51 (m, 6H, Ar-H), 7.43 (d, 1H, Ar-H), 7.38 (d, 1H, Ar-H) ppm.  $^{13}\text{C}$  NMR (100 MHz, DMSO- $d_6$ ):  $\delta$  158.98 (coumarin C=O), 146.86, 145.50, 143.75, 142.72, 140.91, 138.91, 137.39, 132.37, 132.21, 131.08, 129.61, 128.92,

128.81, 127.21, 127.08, 126.91, 124.68, 120.98 ppm. MS-EI, ( $m/z$ ): = 367 [M=2], 365 [M];  
Anal. For C<sub>19</sub>H<sub>12</sub>ClN<sub>3</sub>O<sub>3</sub>: calcd. C, 62.39; H, 3.31; N, 11.49; Found: C 62.41, H 3.35, N 11.53.

**3-(6-Bromo-2-oxo-2H-chromen-3-yl)-1-(4-bromophenyl)-1H-pyrazole-4-oxime (5d)**

Yield: 78%, colour: Light brown. MP = 277-279 °C (dec.). IR (KBr,  $\nu_{\max}$ , cm<sup>-1</sup>): 1737 (coumarin, C=O), 3445 (-OH). <sup>1</sup>H NMR (400 MHz, DMSO-d<sub>6</sub>):  $\delta$  9.09 (s, 1H, pyrazole, C-H), 8.80 (s, 1H, coumarin C<sub>4</sub>-H), 8.36 (d, 1H, Ar-H), 8.06 (s, 1H, Ar-H), 7.93-7.64 (m, 4H, Ar-H), 7.55 (d, 1H, Ar-H), 7.40 (d, 1H, Ar-H), 7.36 (d, 1H, Ar-H) ppm. <sup>13</sup>C NMR (100 MHz, DMSO-d<sub>6</sub>):  $\delta$  159.37 (coumarin C=O), 153.42, 146.88, 145.52, 143.75, 142.72, 140.91, 138.91, 137.39, 132.37, 132.21, 131.08, 129.61, 128.92, 128.82, 127.21, 127.08, 126.90, 124.68, 120.96 ppm. MS-EI, ( $m/z$ ): = 490 [M+4], 488 [M+2], 486 [M]; Anal. For C<sub>19</sub>H<sub>11</sub>Br<sub>2</sub>N<sub>3</sub>O<sub>3</sub>: calcd. C, 46.66; H, 2.27; N, 8.59; Found: C 46.69, H 2.30, N 8.61.

**3-(2-Oxo-2H-chromen-3-yl)-1-phenyl-1H-pyrazole-4-carbonitrile (6a)**

Yield: 89%, colour: pale yellow. MP = 212-214 °C. IR (KBr,  $\nu_{\max}$ , cm<sup>-1</sup>): 1726 (coumarin, C=O), 1602 (pyrazole, C=N), 2224 (Nitrile). <sup>1</sup>H NMR (400 MHz, DMSO-d<sub>6</sub>):  $\delta$  9.44 (s, 1H, pyrazole, C-H), 8.56 (s, 1H, coumarin C<sub>4</sub>-H), 7.94 (d, 1H, Ar-H), 7.90 (d, 1H, Ar-H), 7.88 (d, 1H, Ar-H), 7.73 (t, 1H, Ar-H), 7.61 (t, 1H, Ar-H), 7.51- 7.41 (m, 4H, Ar-H) ppm. MS-EI, ( $m/z$ ): = 313 [M+1]; Anal. For C<sub>19</sub>H<sub>11</sub>N<sub>3</sub>O<sub>2</sub>: calcd. C 72.84, H 3.54, N 13.41; Found: C 72.90, H 3.61, N 13.49.

**1-(4-Chlorophenyl)-3-(2-oxo-2H-chromen-3-yl)-1H-pyrazole-4-carbonitrile (6b)**

Yield: 72%, colour: White. MP = 198-200 °C. IR (KBr,  $\nu_{\max}$ , cm<sup>-1</sup>): 1721 (coumarin, C=O), 1601 (pyrazole, C=N), 2218 (Nitrile). <sup>1</sup>H NMR (400 MHz, DMSO-d<sub>6</sub>):  $\delta$  8.73 (s, 1H, pyrazole, C-H), 8.70 (s, 1H, coumarin C<sub>4</sub>-H), 8.05 (d, 1H, Ar-H), 7.79 (d, 1H, Ar-H), 7.76 (d, 1H, Ar-H), 7.72-7.14 (m, 4H, Ar-H), 7.08 (t, 1H, Ar-H), ppm. <sup>13</sup>C NMR (100 MHz, DMSO-d<sub>6</sub>):  $\delta$  161.59

(coumarin C=O), 156.46, 151.83, 151.67, 151.61, 144.91, 144.12, 139.20, 134.49, 133.87, 132.62, 131.98, 129.01, 128.80, 128.39, 122.48, 120.58 ppm. MS-EI, ( $m/z$ ): = 349 [M+2], 347 [M]; Anal. For C<sub>19</sub>H<sub>10</sub>ClN<sub>3</sub>O<sub>2</sub>: calcd. C, 65.62; H, 2.90; N, 12.08; Found: C 65.66, H 2.94, N 12.12.

***1-(4-Bromophenyl)-3-(2-oxo-2H-chromen-3-yl)-1H-pyrazole-4-carbonitrile (6c)***

Yield: 78%, colour: Light brown. MP = 220-222 °C. IR (KBr,  $\nu_{\max}$ , cm<sup>-1</sup>): 1731 (coumarin, C=O), 1601 (pyrazole, C=N), 2223 (Nitrile). <sup>1</sup>H NMR (400 MHz, DMSO-d<sub>6</sub>):  $\delta$  9.44 (s, 1H, pyrazole, C-H), 8.57 (s, 1H, coumarin C<sub>4</sub>-H), 7.97 (d, 1H, Ar-H), 7.88 (d, 1H, Ar-H), 7.73 (d, 1H, Ar-H), 7.71-7.49 (m, 4H, Ar-H), 7.43 (t, 1H, Ar-H), ppm. <sup>13</sup>C NMR (100 MHz, DMSO-d<sub>6</sub>):  $\delta$  158.21 (coumarin C=O), 153.50, 148.20, 143.55, 138.20, 135.92, 133.01, 129.72, 129.30, 128.13, 124.95, 119.45, 118.53, 117.81, 116.19, 112.95, 93.95 ppm. MS-EI, ( $m/z$ ): = 393 [M+2], 391 [M]; Anal. For C<sub>19</sub>H<sub>10</sub>BrN<sub>3</sub>O<sub>2</sub>: calcd. C, 58.18; H, 2.57; N, 10.71; Found: C 58.21, H 2.62, N 10.74.

***3-(6-Bromo-2-oxo-2H-chromen-3-yl)-1-(4-bromophenyl)-1H-pyrazole-4-carbonitrile (6d)***

Yield: 75%, colour: Brown. MP = 187-189 °C. IR (KBr,  $\nu_{\max}$ , cm<sup>-1</sup>): 1731 (coumarin, C=O), 1600 (pyrazole, C=N), 2224 (Nitrile). <sup>1</sup>H NMR (400 MHz, DMSO-d<sub>6</sub>):  $\delta$  9.91 (s, 1H, pyrazole, C-H), 9.26 (s, 1H, coumarin C<sub>4</sub>-H), 8.39 (d, 1H, Ar-H), 8.12 (d, 1H, Ar-H), 7.98 (d, 1H, Ar-H), 7.96-7.42 (m, 4H, Ar-H), ppm. <sup>13</sup>C NMR (100 MHz, DMSO-d<sub>6</sub>):  $\delta$  162.50 (coumarin C=O), 159.20, 151.66, 150.73, 144.91, 144.12, 142.68, 139.28, 134.89, 132.73, 130.00, 129.73, 127.87, 122.48, 120.58, 119.67, 118.49 ppm. MS-EI, ( $m/z$ ): = 393 [M+2], 391 [M]; Anal. For C<sub>19</sub>H<sub>9</sub>Br<sub>2</sub>N<sub>3</sub>O<sub>2</sub>: calcd. C, 48.44; H, 1.93; N, 8.92; Found: C 48.47, H 1.96, N 8.97.

***3-(1-Phenyl-4-(1H-tetrazol-5-yl)-1H-pyrazol-3-yl)-2H-chromen-2-one (7a)***

Yield: 84%, colour: yellow. MP = 284-285 °C (dec.). IR (KBr,  $\nu_{\max}$ ,  $\text{cm}^{-1}$ ): 1726 (coumarin, C=O), 1606 (pyrazole, C=N), 3428 (Tetrazole, N-H).  $^1\text{H}$  NMR (400 MHz, DMSO- $d_6$ ):  $\delta$  9.18 (s, 1H, tetrazole, N-H), 8.47 (s, 1H, pyrazole, C-H), 7.99 (s, 1H, coumarin C<sub>4</sub>-H), 7.89 (d, 2H, Ar-H), 7.86 (d, 1H, Ar-H), 7.70 (t, 1H, Ar-H), 7.58 (t, 1H, Ar-H), 7.48 (d, 1H, Ar-H), 7.45 (t, 1H, Ar-H), 7.43 (t, 1H, Ar-H), 7.41 (t, 1H, Ar-H) ppm.  $^{13}\text{C}$  NMR (100 MHz, DMSO- $d_6$ ):  $\delta$  164.24 (coumarin C=O), 162.00 (tetrazole C<sub>4</sub>), 158.73 (coumarin C-O), 153.53, 145.57, 143.24, 138.71, 132.50, 129.74, 128.97, 127.50, 124.80, 119.00, 116.15, 115.97, 113.21, 110.11 (pyrazole C<sub>3</sub>) ppm. MS-EI, ( $m/z$ ): = 356 [M+1]; Anal. For C<sub>19</sub>H<sub>12</sub>N<sub>6</sub>O<sub>2</sub>: calcd. C 64.04, H 3.39, N 23.58; Found: C 64.09, H 3.46, N 23.67.

**6-Chloro-3-(1-phenyl-4-(1H-tetrazol-5-yl)-1H-pyrazol-3-yl)-2H-chromen-2-one (7b)**

Yield: 82%, colour: yellow. MP = 280-282 °C (dec.). IR (KBr,  $\nu_{\max}$ ,  $\text{cm}^{-1}$ ): 1720 (coumarin, C=O), 1606 (pyrazole, C=N), 3224 (tetrazole, N-H).  $^1\text{H}$  NMR (400 MHz, DMSO- $d_6$ ):  $\delta$  9.22 (s, 1H, tetrazole, N-H), 8.43 (s, 1H, pyrazole, C-H), 8.00 (d, 1H, Ar-H), 7.97 (s, 1H, Ar-H), 7.95 (s, 1H, Ar-H), 7.74 (d, 1H, Ar-H), 7.61-7.53 (m, 4H, Ar-H), 7.43 (t, 1H, Ar-H) ppm.  $^{13}\text{C}$  NMR (100 MHz, DMSO- $d_6$ ):  $\delta$  162.03 (coumarin C=O), 160.12 (tetrazole C<sub>4</sub>), 158.30 (coumarin C-O), 152.15, 145.24, 141.95, 138.66, 132.03, 129.78, 128.50, 127.94, 127.59, 120.32, 119.01, 118.20, 114.08, 110.15 (pyrazole C<sub>3</sub>) ppm. MS-EI, ( $m/z$ ): = 392 [M+2], 390 [M]; Anal. For C<sub>19</sub>H<sub>11</sub>N<sub>6</sub>ClO<sub>2</sub>: calcd. C 58.40, H 2.84, N 21.51; Found: C 58.47, H 2.90, N 21.62.

**6-Bromo-3-(1-phenyl-4-(1H-tetrazol-5-yl)-1H-pyrazol-3-yl)-2H-chromen-2-one (7c)**

Yield: 72%, colour: pale brown. MP = 272-274 °C (dec.). IR (KBr,  $\nu_{\max}$ ,  $\text{cm}^{-1}$ ): 1726 (coumarin, C=O), 1610 (pyrazole, C=N), 3123 (tetrazole, N-H).  $^1\text{H}$  NMR (400 MHz, DMSO- $d_6$ ):  $\delta$  9.15 (s, 1H, tetrazole, N-H), 8.45 (s, 1H, pyrazole, C-H), 7.95 (d, 1H, Ar-H), 7.84 (s, 1H, Ar-H), 7.65 (d, 1H, Ar-H), 7.57 (d, 1H, Ar-H), 7.47-7.38 (m, 5H, Ar-H) ppm.  $^{13}\text{C}$  NMR (100 MHz, DMSO- $d_6$ ):

$\delta$  161.61 (coumarin C=O), 159.37 (tetrazole C<sub>4</sub>), 155.08 (coumarin C-O), 146.15, 143.87, 139.24, 133.13, 130.35, 130.24, 129.57, 128.12, 126.01, 125.43, 120.73, 119.56, 116.75, 108.88 (pyrazole C<sub>3</sub>) ppm. MS-EI, ( $m/z$ ): = 436 [M+2], 434 [M]; Anal. For C<sub>19</sub>H<sub>11</sub>N<sub>6</sub>BrO<sub>2</sub>: calcd. C 52.43, H 2.55, N 19.31; Found: C 52.51, H 2.60, N 19.38.

**6-Bromo-3-(1-(4-bromophenyl)-4-(1H-tetrazol-5-yl)-1H-pyrazol-3-yl)-2H-chromen-2-one (7d)**

Yield: 70%, colour: brown. MP = 272-274 °C (dec.). IR (KBr,  $\nu_{\max}$ , cm<sup>-1</sup>): 1726 (coumarin, C=O), 1606 (pyrazole, C=N), 3123 (tetrazole, N-H). <sup>1</sup>H NMR (400 MHz, DMSO-d<sub>6</sub>):  $\delta$  9.18 (s, 1H, tetrazole, N-H), 8.41 (s, 1H, pyrazole, C-H), 7.98 (d, 2H, Ar-H), 7.94 (s, 1H, Ar-H), 7.72 (d, 2H, Ar-H), 7.50 (d, 2H, Ar-H), 7.40 (s, 1H, Ar-H) ppm. <sup>13</sup>C NMR (100 MHz, DMSO-d<sub>6</sub>):  $\delta$  162.87 (coumarin C=O), 158.92 (tetrazole C<sub>4</sub>), 154.22 (coumarin C-O), 152.70, 145.79, 142.56, 139.18, 132.64, 130.38, 129.09, 128.51, 128.21, 121.90, 120.89, 119.56, 118.80, 105.06 (pyrazole C<sub>3</sub>) ppm. MS-EI, ( $m/z$ ): = 516 [M+4], 514 [M+2], 512 [M]; Anal. For C<sub>19</sub>H<sub>10</sub>N<sub>6</sub>Br<sub>2</sub>O<sub>2</sub>: calcd. C 44.39, H 1.96, N 16.35; Found: C 44.45, H 1.99, N 16.42.

## RESULTS AND DISCUSSION

The conversion of coumarin pyrazolonitriles **6(a-d)** to tetrazoles **7(a-d)** was confirmed through IR spectra which showed disappearance of CN absorption band around 2224-2236 cm<sup>-1</sup> and appearance of new band in the range 3426-3450 cm<sup>-1</sup> due to N-H and also compounds have shown strong adsorption band for carbonyl carbon of coumarin and tetrazole (N-H) at 1720-1727 and 3224-3428 cm<sup>-1</sup>, respectively. The <sup>1</sup>H NMR spectrum of showed a singlet at  $\delta$  9.17-9.29, 7.74-7.99 and 8.40-8.51 ppm. due to N-H of tetrazole, C<sub>4</sub>-H of coumarin and pyrazole ring proton, respectively. Aromatic protons in all compounds appeared as multiplets in the range 7.59-7.68 to 7.28-7.54 ppm. Further, <sup>13</sup>C NMR spectral study indicated the number of signals in consistent with number of magnetically non equivalent carbon atoms and also in mass spectra all

the synthesised compounds have shown the molecular ion peaks at their respective m/z values (representative spectra are given in Supporting Information, Figs. S1-S51).

Subsequently, the X-ray diffraction structures of novel dyes **7b** and **7c** were obtained. Both structures were obtained by using DMSO (HPLC grade) at room temperature and obtained single crystal structure of the compound is characterized by a long range, well defined three dimensional orders. The asymmetric unit of the enantiotopic structure of the compound is shown in Fig. 2. These dyes crystallize in the monoclinic  $P2_1$  space group. Both the compounds crystallize in the same asymmetric space groups. In the refined structure, all bond lengths and angles are within normal ranges (26) (Supporting Information, Table S52).

#### Crystal Data for Compound **7b**:

$C_{19}H_{11}ClN_6O_2$ , ( $M = 390.79$  g/mol): Monoclinic, space group  $P2_1$  (no. 4),  $a = 6.2282(5)$  Å,  $b = 19.8260(14)$  Å,  $c = 15.5480(12)$  Å,  $\beta = 92.283(5)^\circ$ ,  $V = 1918.3(3)$  Å<sup>3</sup>,  $Z = 4$ ,  $T = 296.15$  K,  $\mu(\text{MoK}\alpha) = 0.226$  mm<sup>-1</sup>,  $D_{\text{calc}} = 1.353$  g/cm<sup>3</sup>, 18814 reflections measured ( $3.33^\circ \leq 2\theta \leq 56.964^\circ$ ), 8338 unique ( $R_{\text{int}} = 0.0353$ ,  $R_{\text{sigma}} = 0.0566$ ) which were used in all calculations. The final  $R1$  was 0.0427 ( $I > 2\sigma(I)$ ) and  $wR2$  was 0.0907.

#### Crystal Data for Compound **7c**:

$C_{19}H_{11}BrN_6O_2$ , ( $M = 435.25$  g/mol): monoclinic, space group  $P2_1$  (no. 4),  $a = 6.2436(4)$  Å,  $b = 19.8399(12)$  Å,  $c = 15.6428(10)$  Å,  $\beta = 92.017(3)^\circ$ ,  $V = 1936.5(2)$  Å<sup>3</sup>,  $Z = 4$ ,  $T = 296.15$  K,  $\mu(\text{MoK}\alpha) = 2.150$  mm<sup>-1</sup>,  $D_{\text{calc}} = 1.493$  g/cm<sup>3</sup>, 14713 reflections measured ( $3.316^\circ \leq 2\theta \leq 52.432^\circ$ ), 6778 unique ( $R_{\text{int}} = 0.0300$ ,  $R_{\text{sigma}} = 0.0654$ ) which were used in all calculations. The final  $R1$  was 0.0386 ( $I > 2\sigma(I)$ ) and  $wR2$  was 0.0885.

< Fig. 2 >

#### Hirshfeld surface determination for compound **7b** and **7c**

Molecular Hirshfeld surfaces in the crystal structure are constructed basing on the electron distribution calculated as the sum of spherical atom electron densities. For a given crystal structure the Hirshfeld surface is unique and this property helps further gain additional insight into the intermolecular interaction of molecular crystals. For each point on that isosurface, two distances are defined:  $d_e$ , the distance from the point to the nearest nucleus external to the surface, and  $d_i$  is the distance to the nearest nucleus internal to the surface. The normalized contact distance ( $d_{norm}$ ) based on both  $d_e$  and  $d_i$ , and the Van-der-Waals (vdW) radii of the atom, is given by the Eq. (1), which enables us to identify the regions of particular important intermolecular interactions.

$$d_{norm} = \frac{[d_i - r_i^{vdW}]}{r_i^{vdW}} + \frac{[d_e - r_e^{vdW}]}{r_e^{vdW}} \quad (1)$$

From Eq. (1),  $r^{vdW}$  represents the Van Der Waals (vdW) radius of the appropriate atom internal or external to the surface.  $d_{norm}$  is negative where contacts shorter than vdW separations and positive for contacts greater than vdW separations, which are displayed using a red-white-blue color scheme. The red regions correspond to closer contacts with negative  $d_{norm}$  value, the blue regions correspond to longer contacts with positive  $d_{norm}$  value and the white regions correspond to the  $d_{norm}$  value of zero (contacts around the vdW separation). Short contacts were observed with larger and brighter red spots as inter nuclear separations ( $d_i$  and  $d_e$ ) decreases. Since  $d_{norm}$  is symmetric in  $d_i$  and  $d_e$ , any close intermolecular contacts are characterized by two identical red regions. One act as a donor and another as an acceptor if  $d_i < d_e$  or  $d_i > d_e$  respectively (27). The combination of  $d_e$  and  $d_i$  in the form of a 2D fingerprint plot provides summary of intermolecular contacts in the crystal. In addition, crystal voids were generated by plotting the isosurface at 0.002 au for the entire procrystal electron density.

The Hirshfeld surfaces mapped with  $d_{\text{norm}}$  and Shape index are shown in Fig. 3. The 3-D  $d_{\text{norm}}$  surfaces were mapped by using a fixed color scale of 0.223 (red) to 1.411 Å (blue) and Shape index were mapped in the color range of  $\pm 1.000$  Å. As we expected, the  $d_{\text{norm}}$  surfaces shown in Fig. 3 a, b reveal the close contacts of hydrogen bond donors and acceptors, but other close contacts are also evident here. In  $d_{\text{norm}}$  surfaces, for both compounds **7b** and **7c**, the large circular depressions (deep red) are the indicators of hydrogen bonding contacts, which are due to N-H...N close contacts, whereas other visible light red spots are due to O-H...O contacts. We have identified six and eight intermolecular interactions for compounds **7b** and **7c**, respectively, which are tabulated in Table S53. These interactions stabilize the crystal structure of the compounds.

The Shape index is a qualitative measure of shape. One important attribute of the Shape index is that two shapes where the Shape index differs only by a sign representing complementary "stamp" and "mould" pairs. These maps of Shape index on the Hirshfeld surfaces were used to identify complementary hollows and bumps. The pattern of red and blue triangles on the same region of the shape index surface (Fig. 3 c, d) is characteristic of  $\pi - \pi$  stacking interactions. The pattern of red and blue triangles on this region of both sides of the molecule shows how adjacent molecules in the crystal are related by symmetry. Blue triangles represent convex regions due to ring carbon atoms of the molecule inside the surface, while red triangles represent concave regions due to carbon atoms of the  $\pi$  stacked molecule above it (28).

< Fig. 3 >

The relative percentage contributions of the different interactions to the Hirshfeld surface were calculated for both the compounds and are depicted in Fig. S54.

Fig. S55 (a-l) gives the percentage of contribution of intermolecular interactions to the total Hirshfeld surface for compounds **7b** and **7c**. The fingerprint plots can be decomposed to

highlight particular atoms pair close contacts (29,30). This decomposition enables separation of contributions from different interaction types, which overlap in the full fingerprint. The Fingerprint plots of compound **7b** and **7c** are almost similar for H...H, N...H, O...H and C...H intercontacts. The intermolecular H...H contacts are predominant in the title compounds **7b** & **7c** and their relative contributions being 25.6% and 25% respectively (Fig. S55 c, d). The N...H/H...N interactions are identified by distinct long spikes (Fig. S55 e, f); the upper left spike (donor) is due to H...N and lower right spike (acceptor) is due to N...H interactions and their contribution to Hirshfeld surface are 8.8% and 10.7% for compound **7b** and 9.3% and 10.5% for compound **7c** respectively. In Fig. S55 g, h, the characteristics wings for both the compounds **7b** & **7c** are due to C-H... $\pi$  interactions and their contributions are 15.6% and 12.4% to their Hirshfeld surfaces, respectively. The O...H/H...O interactions are identified as a small spikes (Fig. S55 i, j); the upper left spike (donor) is due to H...O and lower right spike (acceptor) is due to O...H interactions and their contribution to Hirshfeld surfaces are 6% and 6.3%, respectively. In Fig. S55 k, l, another significant interaction in compound **7b** is Cl...H/H...Cl and its contribution to the Hirshfeld surface is 12.2%. Similarly in compound **7c** the Br...H/H...Br interaction contributes about 11.8% to the total Hirshfeld surface.

The electrostatic potential mapped onto Hirshfeld surface to rationalize intermolecular interactions has been represented in Fig. 4. Here the red region is electronegative, while the blue region is electropositive and both are complementing to each other (31). The electrostatic complementarity can be viewed from Fig. 5. In Fig. 5a, electronegative and electropositive patches are present near nitrogen atom and near hydrogen atom, respectively. Similarly in Fig. 5b, electronegative and electropositive patches near carbon and hydrogen atoms are observed.

< Fig. 4 >

< Fig. 5 >

### **Crystal voids**

The anisotropic properties of the molecular solids are determined equally by the empty spaces as well as the filled ones (32). Voids in the crystal can be defined as the region of empty space between the molecules in the crystal and this empty space is the region which lies outside the normal van der Waals surface area of molecules in the unit cell and within which no nuclei exists. Voids in the crystalline material have been visualized by constructing the (0.002 au) - isosurface of procrystal electron density. This 0.002 au electron density isosurface contains more than 98% of the electronic charge of molecules and identifies the empty space in the crystal by determining the shape and size of molecules. Fig. S56 displays the voids surface of the grown crystals of compound **7b** & **7c**. For compound **7b** & **7c**, the volume of the void was computed to be 224.92 Å<sup>3</sup> and 214.62 Å<sup>3</sup>, while from single crystal XRD analysis, the volume of the unit cell comes out to be 1918.3 Å<sup>3</sup> and 1936.5 Å<sup>3</sup>. Thus the volume occupied by voids is around 11.72% and 11.082% of the unit cell volume. Void volume, surface area and void volume as a percentage of total unit cell volume of grown crystals computed at 0.002 au isosurface have been summarized in Table S57.

### **Thermal and Electrochemical Properties:**

From DSC studies, the phase transition properties of these compounds were analyzed. The DSC curves of **7(a-d)** compounds shows an exothermic shift related to the glass transition temperature ( $T_g$ ) at 94.41, 74.61, 69.19 and 95.32°C. The crystalline materials can be characterized by their glass transition temperature ( $T_g$ ). If the material is stored below the  $T_g$ , the rate at which it can recrystallize is significantly reduced relative to a material that is above the glass transition

temperature. Crystallinity of these compounds found a sharp peak at 284.73, 282.02, 274.80°C and 273.89°C. These values are significantly higher than those of other charge transport materials such as the hole transport material N,N'-bis(3-methylphenyl)-N,N'-diphenylbenzidine ( $T_g = 65$  °C) (33). The glass transition temperature of compounds **7a**, **7b**, and **7c** shows an exothermic melting peak at around 74.61 to 95.32°C. However, compound **7d** has shown broad spectrum of recrystallization at 273.89°C with  $T_g$  equal to 69.19 °C which has been detected in thermogram. The exothermic peaks of **7 (a-d)** were observed at higher temperature resulting from recrystallization and it revealed that these compounds are crystalline in nature with good glass transition state stability. In TGA, high thermo-chemical stability of the compounds is demonstrated as shown in Fig. 6 a, b. The thermal decomposition under nitrogen starts above 273-285°C and the temperature for 5% weight loss ( $T_{5d}$ ) were observed at a heating rate of 10°C/min. From all these results it is clear that the studied dyes exhibit good thermal stability (33).

< Fig. 6 >

Further, in order to understand the electro-chemical properties of dyes, we performed CV measurements shown in Fig. 7, calculated HOMO-LUMO and energy band gap of these compounds which are tabulated in Table 1. Band gap of these dyes were calculated from the difference between HOMO and LUMO energy levels. The HOMO-LUMO energy levels were computed using Eq. (2) and (3), respectively by measuring the redox potentials  $E_{red}$  and  $E_{ox}$  and ferrocene is used as the known reference (34).

$$\text{HOMO} = - [ E_{ox}^{onset} + 4.8 ] \text{ (eV)} \quad (2)$$

$$\text{LUMO} = [\text{HOMO} + E_{\text{g}}^{\text{opt}}] \text{ (eV)} \quad (3)$$

Where,  $E_{\text{ox}}^{\text{onset}}$  and  $E_{\text{red}}^{\text{onset}}$  are respectively, measured oxidation and reduction potentials relative to Ag/Ag<sup>+</sup>. From Table 1, it is clear that all **7(a-d)** compounds are possessing almost same energy band gap ranging from 3.95 to 4.03 eV. This is due to the presence of electron withdrawing groups (halogens) on tetrazole linked to pyrazoline coumarin which simultaneously affects both HOMO and LUMO levels and keeping the almost constant difference between HOMO-LUMO (energy band gap) of corresponding dyes. Therefore, the substitution of tetrazole linked pyrazoline derivatives of coumarin has affected both the ground and excited states. These results revealed the oxidation behaviour and hence they can be applied as bipolar transport materials for electroluminescence applications.

< Table 1 >

< Fig. 7 >

### **Photophysical studies:**

To study the photophysical properties of **7(a-d)** dyes, we have used optimised concentrations to avoid aggregation and re-absorption of fluorescence by the dye molecules in steady state spectral measurements. The concentrations were of the order of 1-2  $\mu\text{M}$ .

### ***Quantum yield calculation***

The fluorescence quantum yields ( $\Phi$ ) of **7(a-d)** are determined using coumarin 440 (C440) as reference sample by using Eq. (4) (34) and results are summarized in Table 2.

$$\Phi_{dye} = \Phi_{ref} \frac{I_{dye} A_{ref} n_{dye}^2}{I_{ref} A_{dye} n_{ref}^2} \quad (4)$$

where,  $\Phi_{dye}$  and  $\Phi_{ref}$  are the fluorescence quantum yields of the dyes and reference (C440;  $\Phi_{ref} = 0.98$  in ethanol) (35), respectively,  $A_{dye}$  and  $A_{ref}$  are the optical absorbances of the dye and reference samples at the excitation wavelengths,  $I_{dye}$  and  $I_{ref}$  are the integrated emission intensities of the dyes and reference samples,  $n_{dye}$  and  $n_{ref}$  are the refractive indices of the solvents used for the dyes and the reference, respectively. The Fig. 8 shows the typical overlay of absorption and emission spectra of **7a**, **7b**, **7c**, **7d** and **C440** samples. From Table 2, it is observed that appending the tetrazole pyrazole to coumarin moiety resulted in drastically enhanced PL and QY. However, among the studied pyrazole tetrazole coumarin derivatives, Br-substituted (**7c**) at 6<sup>th</sup> position show comparatively high quantum yield (see Table. 2).

< Table 2 >

< Fig. 8 >

### **Optical band gap**

The energy levels of the electronic states correspond to the energy carried by UV or Visible radiation. At resonance, the molecules will absorb quantized energy transported by the electromagnetic radiation and promote an electron from the low energy molecular orbital to higher energy molecular orbital (36). The optical band ( $E_g^{opt}$ ) corresponds to the energy of the long edge wavelength of the exciton absorption band (37). Conversely, the optical band gap values of **7(a-d)** dyes were approximated from the onset of the low energy side of their absorption spectra ( $\lambda_{onset}$ ) to the baseline according to the Eq. (5) (38,39). The calculated optical

$E_g$  values ranging from 3.96 to 4.03 eV as tabulated in Table 1. From this table we noticed that the halide groups at 6<sup>th</sup> position of coumarin appended to tetrazole-pyrazole derivative has no significant effect on  $E_g$ . But as compared to Dipyrazolopyridine derivatives (40), our tetrazole pyrazole coumarin derivatives possessing slightly higher optical energy band gap. And good agreement of their band gaps obtained by the absorption spectrum and CV measurements were observed. And in both measurements, the constant  $E_g$  values of **7(a-d)** noticed and suggested the less prominent effect of substituent (halogens) on  $E_g$ . Also this fact is well supported by DFT study which is discussed in the next section.

$$E_g^{opt} = \frac{1240}{\lambda_{onset}} \quad (5)$$

#### ***Substituent and Solvent Effect:***

With the synthetic dyes in hand, it is most important to investigate effect of substituent on the photophysical properties of dyes. Hence, absorption and fluorescence spectra of **7(a-d)** dyes were recorded in same solvent *viz.*, ethyl acetate (EA) to study the effects of substituent on PL properties and the results are summarized in Table 2 (see Supporting Information, Fig. S58 a, b). From this table, we found that absorption wavelength of **7(b-d)** dyes has been slightly blue shifted relative to **7a** dye. This is due to presence of conjugation in pyrazole linked tetrazole -NH of the coumarin. Further, the corresponding fluorescence emission maxima of **7b**, **7c** and **7d** dyes also have been blue shifted. Therefore, both ground and excited states were affected equally due to the halide functional group at 6<sup>th</sup> position of coumarin of all studied dyes. As a consequence, there is no rapid variation in stokes shift and in turn absence in the variation of energy band gap of corresponding dyes. This result is in consistent with the previously discussed CV and optical band gap measurements.

Now to understand the effects of solvents polarity on PL properties of tetrazole pyrazole coumarin derivatives dyes containing different halogens as substituent were recorded in alcohols (methanol to decanol) and general solvents (DMSO, DMF, Acetonitrile, Chloroform and EA). For instance, the overlay of absorption and emission spectra of dye **7a** is shown in Fig. 9 a, b. From this figure, it is observed that the fluorescence emission maximum of **7a** has red shifted (bathochromic shift) as a function of increasing solvent polarity. Further, the same results were observed for **7(b-d)** dyes (see Figs. S59-S61 and Figs. S62-S64). This is attributed to change in the ground and excited state dipole moments of **7(a-d)** dyes which implies the relative change in ground and excited state energy distribution of these dyes. Comparable shifts observed in absorption and emission spectra show the small difference between ground and excited state dipole moment. These results are also confirmed by DFT studies given in the next section. The bathochromic shift of these dyes is attributed to the interaction of solute molecule with the surrounding solvent environment. Since the solute molecule finds itself in a cavity inside the solvent that results in stabilization of the ground state. The Franck-Condon excited state is formed in a solvent cage of already partly oriented solvent dipoles. The better stabilization of the excited state relative to the ground state with increasing solvent polarity results in a bathochromic shift (positive solvatochromism). It is also apparent from the slight increasing values of dipole moments during the electron transition for dye molecules calculated from DFT studies as given in Table 3 ( $\mu_e > \mu_g$ ). Difference is not to a greater extent, the small change in dipole moment value can be understood based on change in tendency of electron movement from donor to acceptor group. This delocalization of electrons in aromatic ring is also affected by change in the surrounding environment created by solvents of different polarity. Further, observed Stokes shift in alcohols, as tabulated in Table 2 (for general solvents, see Supporting

Information, Table S65), clearly suggested the presence of intramolecular charge transfer (ICT) character in these dyes.

< Table 3 >

< Fig. 9 >

### *Computational studies*

Further, to gain deep insight into the electronic structure and the HOMO–LUMO levels of **7(a-d)** dyes, DFT (B3LYP) calculations were performed. It has been reported that the B3LYP/6-31G level of theory can give reliable geometry parameters of organic dyes. The ICT activities are related to the orbital spatial distribution and the compositions of the frontier molecular orbital.

The HOMO-LUMO structures of **7(a-d)** dyes are shown in Fig. 10. Computationally elaborated electronic properties reveal the nature of HOMO and LUMO levels. The close observation of this figure depicts for all dyes electron density in LUMO concentrated mainly on coumarin moiety linked to different electron withdrawing groups while in HOMO level, electron density distributed over tetrazole moiety. Therefore, all dyes possessed similar HOMO and LUMO levels irrespective of substituent attached to coumarin moiety. Hence, the energy band gaps of all molecules ranging from 3.96 to 4.03 eV.

< Fig. 10 >

< Fig. 11 >

The fluorescence decay lifetimes of dyes were measured using Time Correlated Single Photon Counting (TCSPC) instrument. The instrument utilizes pico second light emitting diode for the excitation generating pulses at 296 nm with instrument response function 851 ps. The fluorescence decays were fitted to tri-exponential functions. The average lifetime,  $\langle \tau \rangle$  is

calculated from Eq. (6) (41) in alcohols and are tabulated in Table 2 (for general solvents see Supporting Information, Table S65).

$$\langle \tau \rangle = \frac{\sum \tau_i \alpha_i}{\sum \alpha_i} \quad (6)$$

where  $\alpha_i$  and  $\tau_i$  are the relative amplitude and lifetime components, respectively. The excitation lifetime profiles in alcohols and general solvents are shown in Supporting Information, Figs. S66-S67 and Figs. S68-S69. However, the fluorescence decay lifetimes profile of **7(a-d)** in ethyl acetate as depicted in Fig. 11 in order to understand the effects of substituent on ICT. From this figure it is clear that the fluorescence decay time was slightly increased from 2.19 to 2.88 ns for **7(a-d)** dyes (see Table 2 for ethyl acetate). This is because the free -NH of tetrazole ring and oxygen atoms in coumarin ring leads to facilitated ICT, which has slightly affected the HOMO-LUMO levels and ground and excited state charge distribution. It is evident from electrostatic potential map (ESP) that the electron cloud mainly localized on coumarin moiety of all derivatives in which red and blue colours are respectively the indicators of high and low electron density as shown in Fig. 12.

< Fig. 12 >

#### *Solvatochromism: Lippert-Mataga considerations*

Ground state and excited state dipole moments for all four compounds are obtained by using Lippert-Mataga equations. Further, difference in the excited state and ground state dipole moments are experimentally calculated. The expression most commonly used in fluorescence spectroscopy is, however, the somewhat simplified equation, first developed by Lippert (42) and Mataga et al. (43). It is based on the Onsager's reaction field theory, the so called Lippert-Mataga equation is no longer applicable when, in addition to the non-specific interactions, specific fluorophore/solvent interactions such as hydrogen bonding or electron-pair

donor/electron-pair acceptor interactions also contribute significantly to the overall solute–solvent interaction. Photophysical parameters from solvatochromism study are presented in Table 4. Kawski and co-workers obtained a simple quantum mechanical second-order perturbation theory of absorption ( $\nu_a$ ) and fluorescence ( $\nu_f$ ) band shifts in different solvents of varying permittivity ( $\epsilon$ ) and refractive index ( $n$ ) relative to the band position of a solute molecule based on which the following equations are obtained.

$$\nu_a - \nu_f = m_1 f(\epsilon, n) + \text{const} \quad (7)$$

$$\nu_a + \nu_f = -m_2 [f(\epsilon, n) + 2g(n)] + \text{const} \quad (8)$$

Where,

$$f(\epsilon, n) = \frac{2n^2 + 1}{n^2 + 2} \left[ \frac{\epsilon - 1}{\epsilon + 2} - \frac{n^2 - 1}{n^2 + 2} \right] \quad (9)$$

is the polarity of solvent and

$$g(n) = \frac{3}{2} \left[ \frac{n^4 - 1}{(n^2 + 2)^2} \right] \quad (10)$$

With

$$m_1 = \frac{2(\mu_e - \mu_g)^2}{hca^3} \quad (11)$$

and

$$m_2 = \frac{2(\mu_e^2 - \mu_g^2)}{hca^3} \quad (12)$$

$h$  being Planck's constant and  $c$  is the velocity of light in vacuum. The parameters  $m_1$  and  $m_2$  can be determined from absorption and fluorescence band shifts [Eqs. (7) and (8)], and the values of  $\mu_g$  and  $\mu_e$  from Eqs. (13) and (14) can be given as,

$$\mu_g = \frac{m_2 - m_1}{2} \left[ \frac{hca^3}{2m_1} \right]^{1/2} \quad (13)$$

$$\mu_e = \frac{m_1 + m_2}{2} \left[ \frac{hca^3}{2m_1} \right]^{1/2} \quad (14)$$

<Table 4 >

The polarity functions graphs for 7a-7d are shown (Figs. S70-S77). These values are now compared with corresponding  $\Delta\mu$  values obtained from theoretical studies. The theoretically evaluated HOMO/LUMO values were discussed and compared with experimentally calculated values from CV studies.

To compute the UV-Vis transition of the compounds, the singlet excited state geometries corresponding to the vertical excitations were optimized using the time dependent DFT (TD-DFT) scheme starting with the ground state geometries optimized in gas phase (44,45). In order to understand the nature of the underlying excited states involved in the experimental absorption spectra, theoretical calculations are essential. The energy of each excited state is the vertical excitation energy in electron volts (eV) from the ground state. The TD-DFT calculations for the compounds were performed by using B3LYP/6-31G and using triple zeta functions B3LYP/6-31G\*. And also the results were checked against the functional dependence by using CAM-B3LYP and B3PWM91 functional. The calculated spin-allowed lowest-energy absorption bands are obtained in the visible region for the studied four basis sets namely B3LYP/6-31G, B3LYP/6-31G\*, CAM-B3LYP/6-31G\* and B3PWM91/ 6-31G\*. The results are tabulated in the **Table 5**. For example, for B3LYP/6-31G basis set at 447 (2.77eV), 446 (2.78eV), 438 (2.76eV) and 428nm (2.86eV), for 7a, 7b, 7c and 7d, respectively. These spin allowed transitions corresponds to an HOMO/LUMO excitation. The corresponding oscillator strengths (f) for 7a,

7b, 7c and 7d are 0.177, 0.184, 0.186 and 0.221, respectively. These results reflect that upon substitution of compound **7a** by different halogens (-Cl, -Br and dibromo), the difference between HOMO and LUMO levels are slightly shortening. These experimental results are in good agreement with theoretically obtained data from DFT studies.

## CONCLUSIONS

In summary, fluorescent dyes 3-(1-aryl-4-(2*H*-tetrazol-5-yl)-1*H*-pyrazol-3-yl)-2*H*-chromen-2-ones **7(a-d)** were designed and synthesized by simple synthetic protocol. Then successfully established their spectroscopic, Hirshfeld Surface, thermal and electronic behaviours from steady state, time resolved, DSC, TGA, CV, and DFT (TD-DFT) studies. Appending the tetrazole pyrazole to coumarin moiety resulted in drastically enhanced PL and QY. Both ground and excited states were affected equally due to the halide functional group at 6<sup>th</sup> position of coumarin of all studied dyes. Hence, there is no rapid variation in stokes shift and energy band gap of corresponding dyes. Therefore,  $E_g$  of **7(a-d)** dyes calculated from DFT, CV and  $\lambda_{onset}$  method are all well matched. However, fluorescence emission maxima of **7(a-d)** has been red shifted (bathochromic shift) as a function of increasing solvent polarity. All these results revealed that chromen-2-one of pyrazoline tetrazole derivatives could be a leading perception for future optoelectronic applications.

**ACKNOWLEDGEMENTS:** The authors are thankful to University Grant Commission (UGC), New Delhi, India for providing financial assistance vide No. F540/2-DSA, 2013 (SAP-I), UGC-UPE (F. No. 14-3/2012 (NS/PE)) and UGC-CPEPA programme (F. No. 8-2/2008 (NS/PE)). Authors are also grateful to the university scientific instrumentation centre (USIC), Karnatak University, Dharwad, for providing the facility to conduct the experiments.

## SUPPORTING INFORMATION

Additional Supporting Information may be found in the online version of this article:

**Figure S1-S51:** IR,  $^1\text{H}$ ,  $^{13}\text{C}$  NMR and Mass spectra for synthesized compounds.

**Table S52:** Obtained main crystallographic parameters.

**Table S53:** Intermolecular interactions with distances for compounds **7b** and **7c**.

**Figure S54:** Relative contributions of various intermolecular contacts to the total Hirshfeld surface for compounds **7b** and **7c**.

**Figure S55: (a-l)** Two dimensional fingerprint plots for the **7b** (shown in **a, c, e, g, i, k**) and compound **7c** (shown in **b, d, f, h, j, l**).

**Table S56:** Different parameters of voids in the crystals.

**Figure S57:** Unit cell voids at (0.002 au) – isosurface.

**Figure S58:** (a) Normalized absorption (left). b) Emission spectra (right) of **7(a-d)** in ethyl acetate.

**Figure S59-S61:** Normalized absorption and emission of **7b, 7c** and **7d** in alcohols.

**Figure S62-S64:** Normalized absorption and emission of **7b, 7c** and **7d** in general solvents.

**Table S65:** Photophysical parameters in general solvents.

**Figure S66-S67:** Fluorescence lifetime profile of **7b, 7c** and **7d** in various alcohols.

**Figure S68-S69:** Fluorescence lifetime profile of **7b, 7c** and **7d** in various GS.

**Figure S70-71:** Polarity function versus Stokes shifts graphs for **7a**.

**Figure S72-73:** Polarity function versus Stokes shifts graphs for **7b**.

**Figure S74-75:** Polarity function versus Stokes shifts graphs for **7c**.

**Figure S76-77:** Polarity function versus Stokes shifts graphs for **7d**.

## REFERENCES

1. Tien-Lin W., C. Ho-Hsiu, H. Pei-Yun, C. Chien-Hong, and L. Rai-Shung (2014) 3,6,9,12-Tetrasubstituted Chrysenes: Synthesis, Photophysical Properties, and Application as Blue Fluorescent OLED. *J. Org. Chem.* **79**, 267-274.
2. Lifen Y., G. Min, N. Daobo, L. Bin, L. Zhiwei, B. Zuqiang, B. H. Jiang and Chunhui (2007) Efficient, saturated red electroluminescent devices with modified pyran-containing emitters. *Optical Materials.* **29**, 1672-1679.
3. Robin SB, Chongen H, Marinus JB, Rob FS, Frans JJdK, Martin L, Anthony L S and Romano VAO (2003) Novel Multicomponent Reaction for the Combinatorial Synthesis of 2-Imidazolines. *Org. Lett.* **5**, 3759-3762.
4. Matthew PA., V. Panos, E. A. C. Adam, R. F. Simon, W. Chung-Tsoi, M. Bassam, L. W. Kai, H. Robert, M. K. Stephen and O. Mary (2005) Linearly polarised organic light-emitting diodes (OLEDs): synthesis and characterisation of a novel hole-transporting photoalignment copolymer. *J. Mater. Chem.* **15**, 3208-3213
5. Sally AS., M. W. Greg, P. C. Jian, Z. Weijie, D. B. Luisa, R. C. Kenneth, R. S. Jesse, V. Reymundo and S. J. Campbell (2003) Stable and Efficient Fluorescent Red and Green Dyes for External and Internal Conversion of Blue OLED Emission. *Chem. Mater.* **15**, 2305-2312.
6. Tarek HE., A. Manuel, C. Raul, M. H. Kassem, M. J. Fadi, M. Lorenzo, S. K. Rony P. Digambara V. T. Tatiana, B. Jean-Luc, J. W. L. Emil, W. Brigitte and R. K. Bilal (2016) Tetraaryl pyrenes: photophysical properties, computational studies, crystal structures, and application in OLEDs. *J. Mater. Chem. C* **4**, 3041-3058.
7. Huda MK and S. K. Dolui (2010) Luminescence property of poly (1,3-bis(phenyl-1,3,4-oxadiazole))s containing polar groups in the main chain. *J. Lumin.* **130**, 2242-2246.

8. Sanjukta, Nad and Haridas, Pal (2001) Unusual Photophysical Properties of Coumarin-151. *J. Phys. Chem. A*, **105**, 1098-1106.
9. Rocío SA., A. S. M Miguel, O. Jaime and Javier FS (2012) Coumarin derivatives for dye sensitized solar cells: a TD-DFT study. *Phys. Chem. Chem. Phys.* **14**, 225-233.
10. Marek C., D. Jana, S. Vojtech, G. Jan, J. Klaudia and G. Anton (2013) 7-(Dimethylamino) coumarin-3-carbaldehyde and Its Phenylsemicarbazone: TICT Excited State Modulation, Fluorescent H-Aggregates, and Preferential Solvation. *J. Phys. Chem. A* **117**, 4870-4883.
11. Mariusz T., K. Dokyoung, S. Subhankar, K. Maciej, H. A. Kyo and T. G. Daniel (2015)  $\pi$ -Expanded coumarins: Synthesis, optical properties and applications. *J. Mater. Chem. C* **3**, 1421-1446.
12. Meryem C., B. Mustafa, K. Mehmet and G. Orhan (2009) Effects of coumarin substituents on the photophysical properties of newly synthesised phthalocyanine derivatives. *Supra. Chem.* **21**, 624-631.
13. Jiang RS., F. Feng, Q. You, G. L. Fu, S. Lin and W. Fu-Hong (2008) A Coumarin-Derived Fluorescence Chemosensors Selective for Copper (II). *Anal. Lett.* **41**, 2203-2213.
14. Sam JB., E. F. Cara, V. F. Rebecca, P. H. Lindsay, A. Michael, J. A. P. Simon, R. R. Craig and T. Riis-Johannessen (2009) Coumarin-based luminescent ligand that forms helicates with dicationic metal ions. *Dalton. Trans.* **47**, 10570-10573.
15. Shridhar IP., B. Ningaraddi, H. R. Mohammed and A. K. Imityyaz (2011) Synthesis and Optoelectronic Properties of Symmetrical Thiophene Based 2,5-disubstituted 1,3,4-oxadiazoles: Highly Fluorescent Materials for OLED Applications. *J. Fluoresc.* **21**, 1515-1519.

16. Mario de la FR., H. A. Clara, F. S. Nerea, B. Gema, G. O. Itxaso, S. David, R. Silvia, R. F. María Isabel (2015) New coumarin-based fluorescent melatonin ligands. Design, synthesis and pharmacological characterization. *Eur. J. Med. Chem.* **103**,370-373.
17. Narahari D., S. B. Ningaraddi, I. P. Shridhar, H. R. Mohammed and A. M. K. Imtiyaz (2014) Synthesis and optoelectronic properties of thieno[2,3-*b*]thiophene based bis 1,3,4-oxadiazole derivatives as blue fluorescent material for use in organic light emitting diodes. *Optical Materials.* **37**, 516-519.
18. Jaehyun L., J. Hyocheol, S. Hwangyu, K. Joonghan, Y. Daisuke, N. Hidetaka, W. Atsushi and P. Jongwook (2016 ) Excimer emission based on the control of molecular structure and intermolecular interactions. *J. Mater. Chem. C* **4**, 2784-2792.
19. Federico A. O RS., D. M. Paula, G. Y. Juan, M. M. Gonzalez, W. Ezequiel, S. Marco, E. B. Rosa and M. C. Franco (2016) Chemical and photochemical properties of chloroharmine derivatives in aqueous solutions. *Phys. Chem. Chem. Phys.* **18**:886-900.
20. Wei C., T. UnSong, Z. Tao, S. Carsten and S. Yu-Fei (2015) Reversible photodimerization of coumarin-modified Wells-Dawson anions. *J. Mater. Chem. C* **3**, 4388-4393.
21. Dolomanov, O.V., L. J. Bourhis, R. J. Gildea, J. A. K. Howard, and H. Puschmann, *OLEX2: a complete structure solution, refinement and analysis program*, (2009), *J. Appl. Cryst.* **42**, 339-341.
22. Sheldrick, (2015) G.M Crystal structure refinement with *SHELXL*, *Acta Cryst.* **A71**, 3-8.
23. Wolff, SK., D. J. Grimwood, J. J. McKinnon, M. J. Turner, D. Jayatilaka, M. A. Spackman. (2012) University of Western Australia.

24. Jayatilaka D and D. J. Grimwood (2003) Applications and Methods-Tonto: A Fortran Based Object-Oriented System for Quantum Chemistry and Crystallography. *Lect. Notes. Comp. Sc.* **2660**, 142-151.
25. Mahadev NK., Ravindra R. K., Atulkumar A. K., Sujith, R. S. K. Sandhya, N. Ramya, K. Guruprasad, K. A. Satish and P. D. Jagadeesh (2016) Design and Microwave Assisted Synthesis of Coumarin Derivatives as PDE Inhibitors. *Intl. J. Med. Chem.* Article ID 9890630, <http://dx.doi.org/10.1155/2016/9890630>.
26. Anthony L. Spek (2009) Structure validation in chemical crystallography. *Acta Cryst.* **65**, 148-155.
27. Christian J., E. Krzysztow, and H. Loic. (2014) The enrichment ratio of atomic contacts in crystals, an indicator derived from the Hirshfeld surface analysis, *International Union of Crystallography (IUCr)*, **1**, 119-128.
28. Spackman M. A and D. Jayatilaka, (2009) Hirshfeld surface analysis. *Cryst. Eng. Comm*, **11**, 19-32.
29. McKinnon J.J., D. Jayatilaka and M.A. Spackman, (2007) Towards quantitative analysis of intermolecular interactions with Hirshfeld surfaces. *Chem. Commun.* **37**, 3814-3816.
30. Spackman M. A and J. J. McKinnon, (2002) Fingerprinting intermolecular interactions in molecular crystals. *Cryst. Eng. Comm.* **4**, 378-392.
31. Spackman M. A., J. J. McKinnon and D. Jayatilaka, (2008) Electrostatic potentials mapped on Hirshfeld surfaces provide direct insight into intermolecular interactions in crystals. *Cryst. Eng. Comm*, **10**, 377-388.
32. Turner MJ., J. J. McKinnon, D. Jayatilaka and M. A. Spackman (2011) Visualisation and characterisation of voids in crystalline materials. *Cryst. Eng. Comm.* **13**, 1804-1813.

33. Manuel WT., H. Bianca, D. Marc, J. Silvia, W. Armin, K. Anna, J. Hans-Hermann and K. Hartmut (2010) Hole-Transporting Host-Polymer Series Consisting of Triphenylamine Basic Structures for Phosphorescent Polymer Light-Emitting Diodes. *J. Polym. Sci. Part A: Polym. Chem.* **48**, 3417-3430.
34. Chung YA., Y. T. Si, W. Shaojue, Q. Qiuyu, F. E. W. Mun, L. Zhong, L. Pei-Zhou, T. S. Subramanian and Z. Yanli (2016) A dual responsive “turn-on” fluorophore for orthogonal selective sensing of biological thiols and hydrogen peroxide. *J. Mater. Chem. C* **4**, 2761-2774.
35. Ashkan S., M. S. Muhamad and Y. Muhammad (2011) Determination of HOMO and LUMO of [6,6]-Phenyl C61-butyric Acid3ethylthiophene Ester and Poly (3-octyl-thiophene-2,5-diyl) through Voltametry Characterization. *Sains. Malaysiana.* **40**, 173-176.
36. Jędrzejewska B., B. Ośmiałowski and R. Zaleśny (2016) Application of spectroscopic and theoretical methods in the studies of photoisomerization and photophysical properties of the push–pull styryl-benzimidazole dyes. *Photochem. Photobiol. Sci.* **15**, 117-128.
37. Ningaraddi SB., D. Narahari, G. H. Pujar, M. N. Wari, S. R. Inamdar and A. M. K. Imtiyaz (2015) Design, Synthesis and Optoelectronic Properties of Unsymmetrical Oxadiazole Based Indene Substituted Derivatives as Deep Blue Fluorescent Materials. *J. Fluoresc.* **25**,1323-1330.
38. Dietrich RTZ., N. G. Gianina and G. Mihaela (2006) The transport gap of organic semiconductors studied using the combination of direct and inverse photoemission. *Chem. Phys.* **325**, 99-112.

39. Patil SK., M. N. Wari, C. Y. Panicker and S. R. Inamdar (2014) Determination of ground and excited state dipole moments of dipolar laser dyes by solvatochromic shift method. *Spectrochim. Acta Mol. Biomol. Spectrosc.* **123**, 117-126.
40. Mahesh K. and S. Karpagam (2016) Synthesis and Optoelectronic Properties of Thiophene Donor and Thiazole Acceptor Based Blue Fluorescent Conjugated Oligomers. *J. Fluoresc.* **26**, 1457-1466.
41. Balasubramaniam ET., Y. T. Danel A., and Tomasik P (2000) Blue Light-Emitting Diodes Based on Dipyrazolopyridine Derivatives. *Chem. Mater.*, **12**, 2788-2793.
42. Lippert E., Z. Naturforsch, Part A (1955) Dipolmoment und Elektronenstruktur von angeregten Molekülen. *J. Phy. Sci.* **10**, 541-545.
43. Mataga N., Y. Kaifu and M. Koizumi, (1956) Solvent Effects upon Fluorescence Spectra and the Dipolemoments of Excited Molecules. *Bull. Chem. Soc. Jpn.* **29**, 465-470.
44. Casida M., (1995) Time dependent density functional response theory for molecules, in Recent Advances in Density Functional Methods, ed. D. P. Chong, *World Scientific, Singapore*, **1**, 155-193.
45. Stratmann RE and Gustavo E. ScuseriaMichael J. Frisch. (1998) An efficient implementation of time-dependent density-functional theory for the calculation of excitation energies of large molecules. *J. Chem. Phys.*, **109**, 8218-8224.

## FIGURE CAPTIONS

**Figure 1.** Photophysical exhibiting structures containing pyrazole and tetrazole scaffolds with emission maxima.

**Figure 2.** Oak Ridge Thermal-Ellipsoid Plot Program (ORTEP) structure of dyes **7b** (panel a) and **7c** (panel b) displacement ellipsoids are drawn at the 50% probability level.

**Figure 3.** Hirshfeld surface mapped with  $d_{\text{norm}}$  (panels a and b) and Shape index properties (panels c and d) for compounds **7b** (panels a and c) and **7c** (panels b and d), are shown. Black colored ellipses on Shape index properties of both compounds represent adjacent red and blue colored triangular surfaces.

**Figure 4.** Electrostatic potential mapped onto Hirshfeld surface using the color range 0.014 (red) and 0.019 (blue) for compounds **7b** (panel a) and **7c** (panel b).

**Figure 5.** Hirshfeld surfaces generated for (a) N $\cdots$ H and (b) C $\cdots$ H intercontacts for compounds **7b** and **7c** with electrostatic potential property mapped on it.

**Figure 6.** (a) DSC curves and (b) TGA thermograms of compounds **7a**, **7b**, **7c** and **7d** deliberated at a rate of heating 10°C min $^{-1}$  under N $_2$ .

**Figure 7.** Cyclic Voltammogram of **7a**, **7b**, **7c** and **7d** in 0.1 M tetrabutylammonium perchlorate in acetonitrile (scan rate: 50.0 mV/s).

**Figure 8.** Overlay of absorption and emission spectra of **7a**, **7b**, **7c** and **7d** and ref **C440** (its structure is shown in right panel) in ethanol at room temperature.

**Figure 9.** (a) Overlay of normalised absorption and emission spectra of **7a** in alcohols; (b) normalised absorption and emission spectra of **7a** in general solvents (see Supporting Information, Figs. S32-S34 for **7b**, **7c** and **7d**).

**Figure 10.** HOMO-LUMO structures for compounds **7a**, **7b**, **7c** and **7d**.

**Figure 11.** Time-resolved fluorescence decay profiles of compound **7a**, **7b**, **7c** and **7d** in *EA*.

**Figure 12.** Optimized ground and excited state molecular structures, and electrostatic potential (ESP) maps of **7a**, **7b**, **7c** and **7d**. Arrows indicate the direction of dipole moment vector.

**Table 1.** Electrochemical data for compound **7a**, **7b**, **7c** and **7d**.

Compound	$E_{\text{ox}}^{\text{onset}}$ <sup>a</sup> (eV)	HOMO <sup>b</sup> (eV)	LUMO <sup>c</sup> (eV)	$E_{\text{g}}$ (eV)	$E_{\text{g}}^{\text{opt}}$ (eV)
<b>7a</b>	0.22	-5.01	-1.03	3.98	3.98
<b>7b</b>	0.22	-5.01	-0.98	4.03	4.03
<b>7c</b>	0.23	-5.03	-1.03	4.00	4.00
<b>7d</b>	0.22	-5.02	-1.07	3.95	3.95

Oxidation potential corresponds to Ag/AgCl electrode, <sup>b</sup> Estimated HOMO from the onset oxidation potentials of the compounds. <sup>c</sup> Calculated using empirical equations (2).

**Table 2.** Summary of quantum yield, optical and thermal behavior of **7a**, **7b**, **7c** and **7d**<sup>a</sup>.

Samples	Solvent	$\lambda_{\max}^{\text{abs}}$ (nm)	$\lambda_{\max}^{\text{em}}$ (nm)	$\Delta\lambda$ (nm)	$\tau_f$ (ns)	$\chi^2$	$\Phi^c$	$T_g/T_c/T_{5d}^d$ (°C)
<b>7a</b>	Methanol	325	417	68	1.26	1.27	0.211	94.41/ 284.73/ 280.00
	Ethanol	325	419	69	1.06	1.27		
	Propanol	325	417	68	1.01	1.27		
	Butanol	325	416	67	1.28	1.25		
	Pentanol	325	415	66	1.23	1.18		
	Hexanol	333	416	60	1.11	1.24		
	Heptanol	315	416	77	1.40	1.26		
	Octanol	333	413	58	1.14	1.28		
	Nonanol	325	412	65	1.33	1.22		
	Decanol	315	412	74	1.25	1.24		
<b>7b</b>	Methanol	348	429	81	3.05	1.24	0.669	74.61/ 282.02/ 278.00
	Ethanol	348	440	92	2.65	1.21		
	Propanol	348	417	69	1.70	1.25		
	Butanol	347	415	68	2.71	1.28		
	Pentanol	331	414	83	1.38	1.11		
	Hexanol	347	417	70	1.80	1.20		
	Heptanol	345	412	67	1.64	1.14		
	Octanol	332	414	82	1.54	1.20		
	Nonanol	332	410	78	1.65	1.17		
	Decanol	332	411	79	1.46	1.24		
<b>7c</b>	Methanol	317	434	117	2.37	1.38	0.870	69.19/ 274.80/ 273.00
	Ethanol	319	430	111	3.71	1.37		
	Propanol	319	423	104	0.78	1.29		
	Butanol	319	420	101	0.62	1.23		
	Pentanol	332	419	87	1.30	1.18		
	Hexanol	333	418	85	0.43	1.13		
	Heptanol	333	417	84	1.08	1.09		
	Octanol	334	417	85	0.75	1.18		
	Nonanol	334	414	80	1.12	1.22		
	Decanol	335	421	86	0.78	1.21		
<b>7d</b>	Methanol	325	417	92	1.27	1.20	0.606	95.32/ 273.89/ 263.00
	Ethanol	325	419	94	1.07	1.17		
	Propanol	325	417	92	1.00	1.16		
	Butanol	325	416	91	1.29	1.17		
	Pentanol	325	415	90	1.23	1.15		
	Hexanol	333	416	83	1.11	1.22		
	Heptanol	315	416	101	1.40	1.29		
	Octanol	333	413	80	1.15	1.23		
<b>C440</b>	Nonanol	325	412	87	1.33	1.12	0.980	-----
	Decanol	315	412	97	1.25	1.31		
	Ethanol	353	429	76	-----	-----		

<sup>a</sup>  $\lambda_{\max}^{\text{abs}}$ : absorption maximum;  $\lambda_{\max}^{\text{em}}$ : emission maximum;  $\Delta\lambda$ : Stokes shift;  $\tau_f$ : fluorescence lifetime;  $\chi^2$ : correlation factor.

**Table 3.** Parameters obtained from DFT studies.

Compounds	HOMO	LUMO	$\Delta E^a$ (eV)	$\mu_g^b$ (Debye)	$\mu_e^c$ (Debye)	$\Delta\mu^d$ (Debye)
<b>7a</b>	-6.135	-2.039	4.095	4.90	6.11	1.21
<b>7b</b>	-6.305	-2.325	3.980	3.58	4.80	0.78
<b>7c</b>	-6.272	-2.283	3.989	3.11	3.91	0.80
<b>7d</b>	-6.348	-2.378	3.969	4.52	6.11	1.59

<sup>a</sup> Band gap,  $\Delta E = \text{HOMO-LUMO}$  (eV); <sup>b</sup>  $\mu_g$  and <sup>c</sup>  $\mu_e$ , are ground and excited state for dipole moments respectively; <sup>d</sup> Difference,  $\Delta\mu = \mu_e - \mu_g$  (Debye)

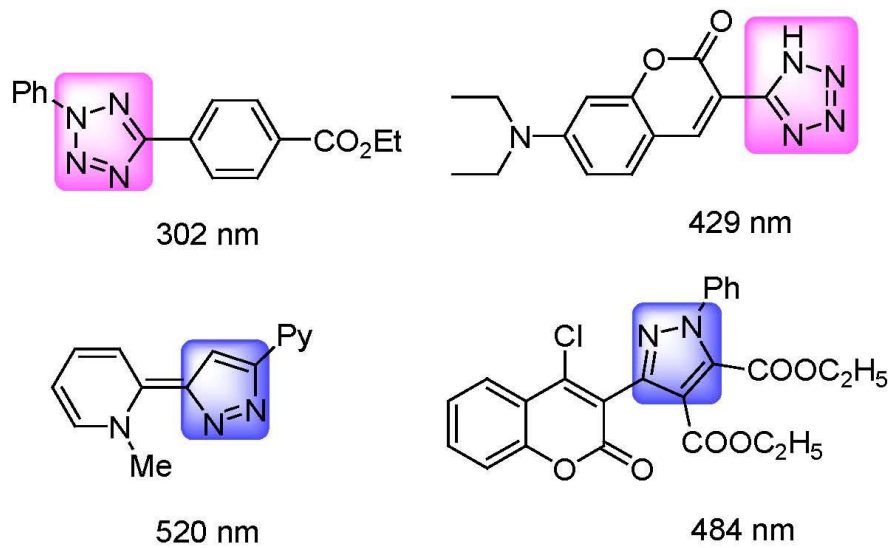
**Table 4.** List of photophysical parameters from solvatochromism study.

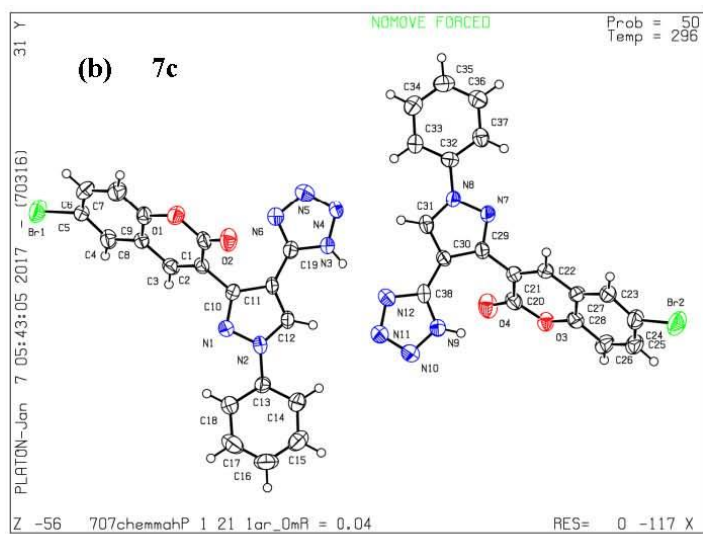
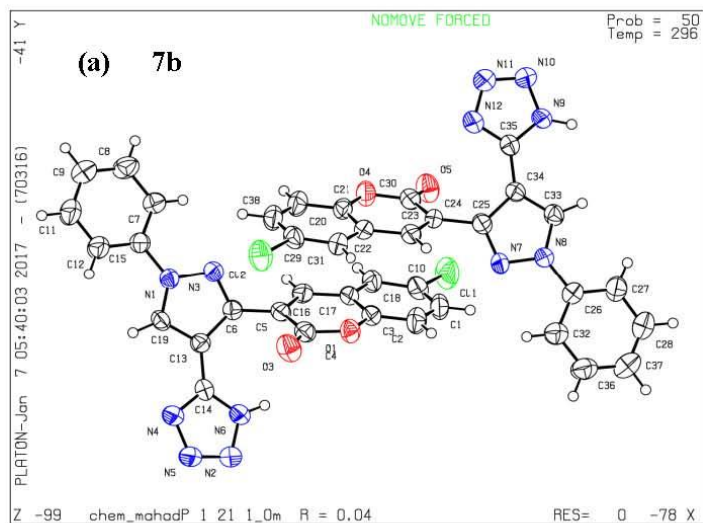
Molecule	Radius ( $\text{\AA}^0$ )	$m_1(\text{cm}^{-1})$	$m_2(\text{cm}^{-1})$	$\mu_g$ (D)	$\mu_e$ (D)	$\Delta\mu$ (D)	$R_1:R_2$
<b>7a</b>	5.60	2041	-9478	4.51	5.82	1.31	0.96:0.94
<b>7b</b>	5.86	6894	-2238	3.89	5.27	1.38	0.91:0.90
<b>7c</b>	5.77	3100	-5184	3.72	4.18	0.46	0.88:0.81
<b>7d</b>	5.71	2689	-9302	4.16	5.93	1.77	0.92:0.91

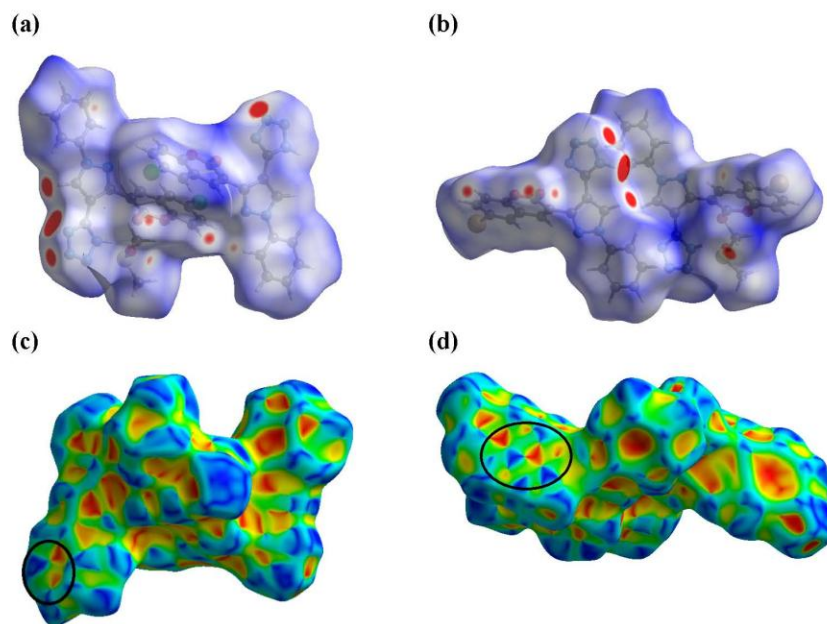
$\mu_g$ : Ground state dipole moment,  $\mu_e$ : Excited state dipole moment,  $\Delta\mu$ : Difference in dipole moment,

**Table 5.** List of important parameters obtained from TD-DFT calculations.

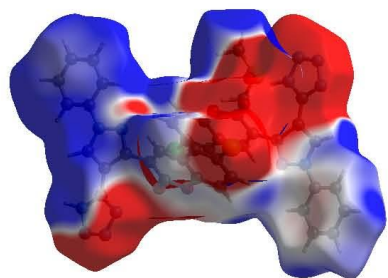
Sample name	Parameter s	TD-DFT			
		B3LYP/6-31G	B3LYP/6-31G*	CAM-B3LYP/6-31G*	B3PW91/6-31G*
<b>7a</b>	$\lambda_{\text{abs}}$ (nm)	447	446	446	446
	E (eV)	2.77eV	2.76	2.76	2.76
	f (Hz)	0.177	0.176	0.176	0.176
<b>7b</b>	$\lambda_{\text{abs}}$ (nm)	446	443	443	443
	E (eV)	2.78eV	2.81	2.81	2.81
	f (Hz)	0.184	0.188	0.188	0.188
<b>7c</b>	$\lambda_{\text{abs}}$ (nm)	438	439	439	439
	E (eV)	2.76eV	2.79	2.79	2.79
	f (Hz)	0.186	0.188	0.188	0.188
<b>7d</b>	$\lambda_{\text{abs}}$ (nm)	428	430	430	430
	E (eV)	2.86eV	2.85	2.85	2.85
	f (Hz)	0.221	0.226	0.226	0.226







(a) 7b



(b) 7c

